Physics of the Earth and Planetary Interiors 276 (2018) 226–233

Contents lists available at ScienceDirect

Physics of the Earth and Planetary Interiors

journal homepage: www.elsevier.com/locate/pepi

Analysis of PKP scattering using mantle mixing simulations and axisymmetric 3D waveforms

Samuel M. Haugland [a,*], Jeroen Ritsema [a], Peter E. van Keken [a,b], Tarje Nissen-Meyer [c]

[a] Department of Earth and Environmental Sciences, University of Michigan, 2534 CC Little, Ann Arbor, MI 48109, USA
[b] Department of Terrestrial Magnetism, Carnegie Institution for Science, 5241 Broad Branch Road NW, Washington, DC 20015, USA
[c] Department of Earth Sciences, University of Oxford, South Parks Road, Oxford OX1 3AN, UK

ARTICLE INFO

Article history:
Received 30 December 2016
Received in revised form 30 March 2017
Accepted 3 April 2017
Available online 6 April 2017

Keywords:
PKIKP precursors
Mantle mixing
Mid-ocean ridge basalt
Wave scattering
Waveform simulation

ABSTRACT

The scattering of PKP waves in the lower mantle produces isolated signals before the PKIKP phase. We explore whether these so-called PKIKP precursors can be related to wave scattering off mid ocean ridge basalt (MORB) fragments that have been advected in the deep mantle throughout geologic time. We construct seismic models of small-scale (>20 km) heterogeneity in the lower mantle informed by mantle mixing simulations from Brandenburg et al. (2008) and generate PKIKP precursors using 3D, axisymmetric waveform simulations up to 0.75 Hz. We consider two end-member geodynamic models with fundamentally different distributions of MORB in the lower mantle. Our results suggest that the accumulation of MORB at the base of the mantle is a viable hypothesis for the origin of PKP scattering. We find that the strength of the PKIKP precursor amplitudes is consistent with P wave speed heterogeneity of 0.1–0.2%, as reported previously. The radial distribution of MORB has a profound effect on the strength of PKIKP precursors. Simulation of PKIKP precursors for models with an increasing MORB concentration in the lowermost 500 km of the mantle appears to reproduce most accurately the strength of PKIKP precursors in Global Seismic Network waveforms. These models assume that MORB has an excess density of at least 7%. Additional simulations of more complex geodynamic models will better constrain the geodynamic conditions to explain the significant variability of PKP scattering strength.

1. Introduction

Upon entry and exit from the core, small-scale heterogeneity in the lower mantle scatters PKP waves. These scattered waves are called PKIKP (or PKP_{df}) precursors because they are recorded up to 20 s before the PKIKP phase between epicentral distances of 120° and 145° (Fig. 1). PKIKP precursors provide some of the best seismic constraints on the nature of kilometer-scale heterogeneity in the lower mantle (see Shearer (2015) for a recent review). Cleary and Haddon (1972) and Haddon and Cleary (1974) first associated PKIKP precursors with wave scattering by small-scale heterogeneity near the core-mantle boundary (CMB). Following these studies a number of researchers have estimated the strength and scale lengths of small-scale heterogeneity responsible for PKP scattering (e.g., Bataille and Flatté, 1988; Hedlin et al., 1997; Shearer et al., 1998; Cormier, 1999; Margerin and Nolet, 2003; Thomas et al., 2009; Mancinelli and Shearer, 2013; Mancinelli et al., 2016), and related PKIKP precursors to CMB topography (e.g., Doornbos, 1978), anomalous low wave speed structures at the base of the mantle (e.g., Vidale and Hedlin, 1998; Wen and Helmberger, 1998; Wen, 2000; Thomas et al., 2009; Frost et al., 2013), and subducted slabs (e.g., Cao and Romanowicz, 2007; Miller and Niu, 2008; Vanacore et al., 2010). Analyses of data from regional (e.g., Thomas et al., 1999; Wen, 2000; Niu and Wen, 2001; Yao and Wen, 2014; Waszek et al., 2015) and global (Hedlin and Shearer, 2000) seismic networks indicate that the amplitudes of PKIKP precursors are highly variable. Hedlin and Shearer (2000) conclude that PKP scattering is relatively strong beneath central Africa, parts of North America, and north of India, while relatively weak beneath South and Central America, eastern Europe, and Indonesia. Given the sparse sampling of the CMB region by PKP, the relationship between the strength of PKP scattering and the large-scale thermal and compositional heterogeneity in the lower mantle, mapped using seismic tomography, remains unclear.

In this study we estimate the strength of PKP scattering assuming that fragments of mid-ocean ridge basalt (MORB) contribute entirely to PKP scattering. These fragments have been continuously generated and dispersed through the mantle by an assumed 4.5 Byr of mixing by mantle convection. The computer simulations of mantle mixing from Brandenburg et al. (2008) inform our models

* Corresponding author.
E-mail address: samhaug@umich.edu (S.M. Haugland).

http://dx.doi.org/10.1016/j.pepi.2017.04.001
0031-9201/

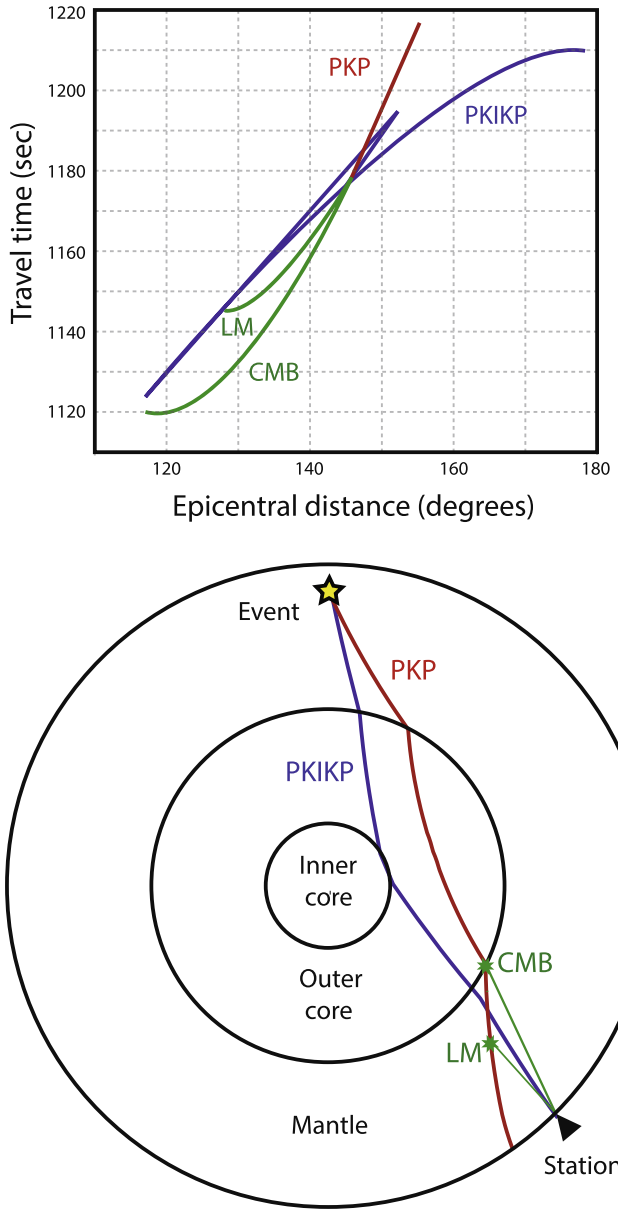

Fig. 1. (top) Travel time curves of (red) PKP, (blue) PKIKP, and (green) PKP scattered waves as a function of traveltime and epicentral distance. Scattering at the core-mantle boundary (labeled CMB) produces the earliest PKIKP precursors. PKP scattering in the lower mantle (labeled LM) is recorded later. (bottom) Ray paths of PKIKP (blue), PKP (red), and two PKP phases that have been scattered at the CMB and in the lower mantle (green). (For interpretation of the references to color in this figure legend, the reader is referred to the web version of this article.)

of MORB concentration in the lower mantle. We relate the MORB fragments to small-scale P wave velocity anomalies and determine the amplitude variations of PKIKP precursors from spectral-element based waveform simulations Nissen-Meyer et al. (2014) at frequencies up to 0.75 Hz. Our hybrid dynamical-seismological approach follows previous joint geodynamic and seismic analyses of wave propagation (Hwang et al., 2011; Styles et al., 2011; Maguire et al., 2016).

2. Seismic data and modeling

2.1. Stacks of Global Seismic Network waveforms

Following the approach of Shearer et al. (1998), Mancinelli and Shearer (2013) and Mancinelli et al. (2016), we quantify the strength of PKP scattering by small-scale heterogeneity in the lower mantle using stacks of about 20,000 globally recorded seismic waveforms (Fig. 2). Events with moment magnitude $M_w \geqslant 5.5$ and hypocenters deeper than 50 km produce the highest quality seismograms. These events are primarily located along the Pacific subduction zones. Most PKP waves cross the CMB beneath the circum-Pacific region. Few PKP waves cross the CMB within the large-low shear velocity provinces in the lower mantle beneath Africa and the Pacific.

The size of our data set, the selection criteria, and signal processing are similar to those in Mancinelli et al. (2016), although we are computationally limited to a narrower frequency band. We filter the waveforms using a band-pass Butterworth filter with corner frequencies of 0.4 Hz and 0.75 Hz and discard records for which the ratio between PKIKP and noise level is lower than 5. The traces are aligned on the arrival times of PKIKP and rescaled such that the amplitude of PKIKP is 1 for all waveforms. We stack the envelopes of all seismograms with common epicentral distances within 0.5° wide epicentral distance bins. We analyze seismograms at epicentral distances between 130° and 140°. This is a slightly narrower range than the distance range of 120°–145° considered by Mancinelli et al. (2016). We prefer the narrower range because PKP_{bc} signals overwhelm synthetic PKIKP precursors at epicentral distances larger than 140° and PKIKP precursors have low amplitudes in the 0.4–0.75 Hz frequency window at epicentral distances smaller than 130°.

Fig. 3 shows the strength of observed PKP scattering. This image shows the amplitude of the stack of waveform envelopes as a function of time and epicentral distance. PKIKP precursors are strongest between 134° and 140°. The time window with precursory signal broadens at distances larger than about 137° but the amplitudes of PKIKP precursors are smaller than 0.1 at more than 7 s before PKIKP. This corresponds to the expected arrival time from heterogeneity near 600 km above the CMB and indicates that the signals of PKP scattering in the lowermost 600 km of the mantle are rela-

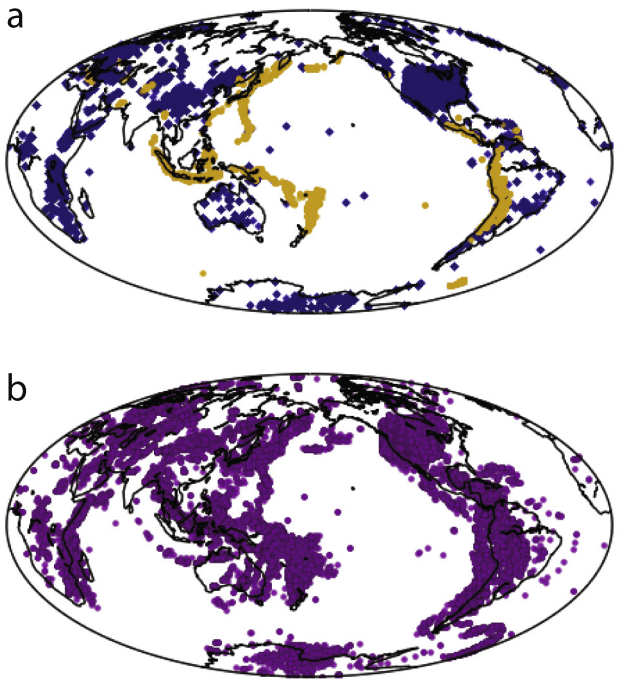

Fig. 2. (a) Location of events since 1990 (orange) and global and regional network stations (blue) used in this study. (b) Location of the core-exit and core-entry points of PKP. (For interpretation of the references to color in this figure legend, the reader is referred to the web version of this article.)

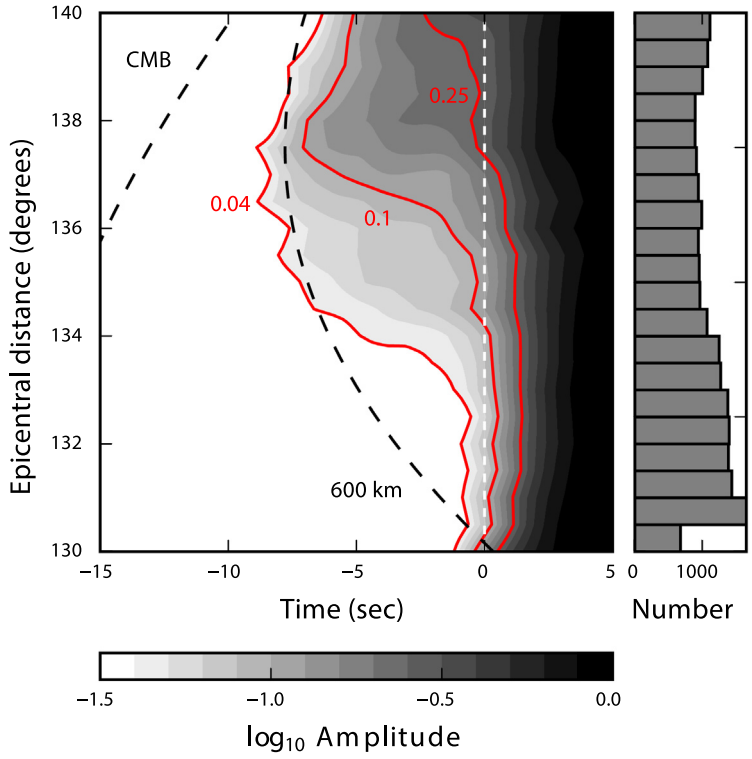

Fig. 3. Amplitude of observed stacked waveform envelopes as a function of epicentral distance shown using a $\log_{10}$ scale. The stacks are determined for recordings within 0.5 increments of epicentral distance. The histogram on the right indicates the number of envelopes contained in each bin. The amplitude of PKIKP is 1. The three red curves are contours where the amplitudes are 0.04, 0.1, and 0.25. The dashed vertical line at time = 0 marks the onset of PKIKP. The dashed curves indicate the ray theoretical onset time of precursors due to scattering at the CMB and at 600 km above the CMB. See Fig. 1 for the absolute travel times.

tively weak in the 0.4–0.75 Hz frequency band, as shown previously by Mancinelli et al. (2016).

2.2. Numerical simulations of mantle mixing

Our models of small-scale heterogeneity in the lower mantle are derived from the numerical simulations of mantle convection in a 2D cylinder by Brandenburg et al. (2008). These numerical models are based on Boussinesq convection at infinite Prandtl number, a thermal Rayleigh number of $Ra = 5 \times 10^6$, with radiogenic internal heating scaled such that it represents present-day heating by radiogenic elements in the Earth's mantle and the estimated effect of present-day secular cooling. The time averaged surface heat flow is similar to the present-day Earth at ≈ 100 mW/m^2. The average surface plate velocity is about 3 cm/yr which is similar to the present-day average poloidal speed of plate tectonics. The models are formulated with a simulated form of plate tectonics using force-balanced plates. This sets up energetically-consistent convection with zones of focused convergence and divergence. At the divergent zones basaltic crust is generated by melting of the mantle peridotite, leaving depleted harzburgite below it. Over time the basalt and harzburgitic components are remixed, but the remnants of oceanic crust (represented by black in the left column of 4) can remain distinctly embedded in the harzburgite. The basalt turns to eclogite and other phases that are assumed to be either neutral in density with the surrounding peridotite or slightly denser. Crust with excess density $\delta\rho > 0$ tends to accumulate near the CMB forming structures similar to the large low shear velocity provinces that are observed in global tomography (e.g., Ritsema et al., 2011). The continuous extraction of oceanic and continental crust leads to a geochemical evolution that is in broad strokes consistent with the observed trace isotope systems and with the degassing efficiency of the Earth as measured by the amount of ^{40}Ar in the Earth's atmosphere.

We choose two simulations (Table 1) from the Brandenburg et al. (2008) study. The MORB concentration C in these simulations have different radial gradients as illustrated in Fig. 5. The geodynamical models assumed a rescaled core radius which leads to a better representation of heat generation and loss compared to the 3D spherical geometry of the Earth (van Keken, 2001). In this study we project the temperature and composition determined by the ratio of MORB and harzburgite back onto a cross-section with Earth-like core radius. Table 1 summarizes the six models that we will analyze. Simulations A and B are horizontal averages of A_1 and A_2 and of B_1 and B_2, respectively. In simulation A, the MORB fragments are passive because they have no excess density (i.e., $\delta\rho = 0\%$). Their concentration is nearly constant with depth. In simulation B, the MORB fragments have an excess density $\delta\rho = +7\%$ and tend to accumulate in the lowermost 500 km of the mantle. We analyze simulations A and B as 1D profiles, ignoring lateral variations of the MORB distribution.

We also analyze the scattering of PKP waves within regions of the mantle characterized by predominantly downwelling or upwelling flow. Sections A_1 and B_1 from simulations A and B isolate

Table 1
Simulations in this study.

Simulation	$\delta\rho$ (%)	Mantle regime
A	0	whole-mantle
A_1	0	downwelling
A_2	0	upwelling
B	+7	whole-mantle
B_1	+7	downwelling
B_2	+7	upwelling

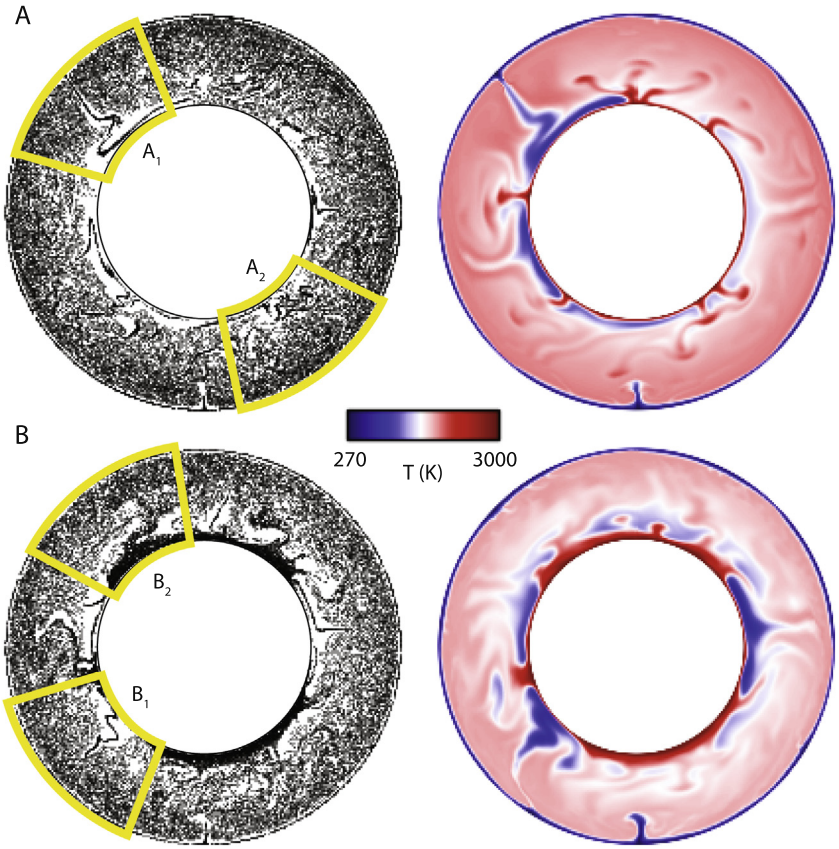

Fig. 4. Mantle cross-section of simulations *A* and *B* from the study by Brandenburg et al. (2008). The panels on the left show tracers that reflect the concentration of MORB. The panels on the right show temperature. Simulations *A* and *B* differ in the assumed excess density $\delta\rho$ of MORB with respect to the mantle. In *A*, $\delta\rho = 0\%$. In *B*, $\delta\rho = +7\%$. The yellow boxes marks regions of the mantle characterized by recent subduction (i.e., A_1 and B_1) or upwelling of the deep mantle (i.e., A_2 and B_2). See also in Table 1.

an episode of recent subduction into the lower mantle. The subducted slab has transported relatively wide sections of oceanic crust to the lowermost mantle which form narrow zones of high MORB concentration. These are visible as spikes in *C* near the CMB in Fig. 5. Sections A_2 and B_2 include upwelling from the CMB. In section B_2, fragments of relatively dense MORB have settled into thick piles above the CMB. The MORB concentration in section B_2 therefore increases faster with depth than in simulation *B* (i.e., the globally averaged MORB structure). On the other hand, the increase in *C* is smaller for section B_1 because MORB fragments have been swept away by recent subduction.

2.3. Waveform simulations

Brandenburg et al. (2008) represented the MORB component by discrete numerical tracers. We use these tracers to define lower mantle small-scale heterogeneity that scatters PKP waves. To reproduce the MORB concentration *C* as a function of depth, we randomly select 25% of the tracers and assume that each tracer has a $20 \times 20\text{km}^2$ volume, the smallest structure to which PKP waves are sensitive at < 0.5 Hz, and a $\delta V_P\%$ higher P velocity than the ambient mantle. The δV_P perturbation is with respect to the P wave velocity and attenuation structure in the Preliminary Reference Earth Model (PREM) at a given depth. Since anomalies may overlap, the seismic anomalies have variable dimensions and spacing and a radial distribution of heterogeneity similar to the MORB distribution in Figs. 4 and 5.

To isolate the effects of wave scattering in the downwelling (i.e., sections A_1 and B_1) and upwelling (i.e., sections A_2 and B_2) regions

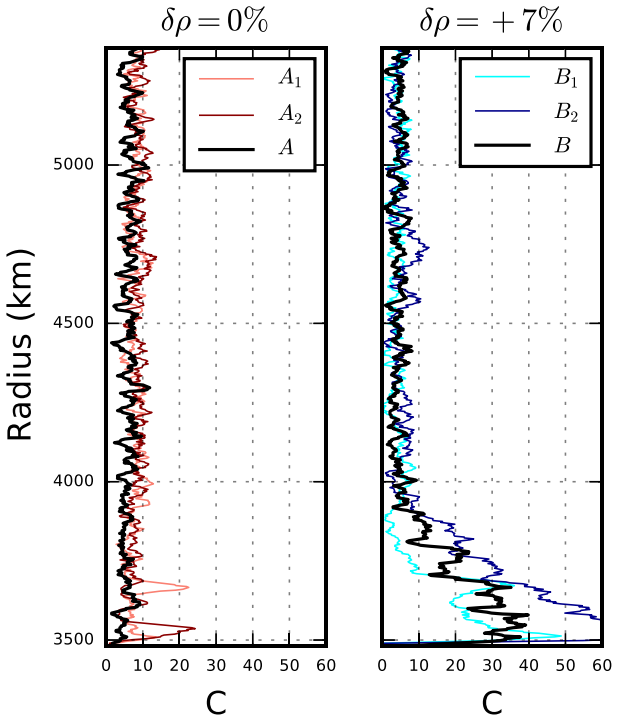

Fig. 5. Profiles of MORB fraction *C* (in %) of the mantle as a function of depth for simulations A, A_1,A_2, B, B_1, and B_2. *C* is defined as the percent mantle volume consisting of MORB tracers in the mantle.

of the mantle, we place P velocity anomalies in the mantle only above the core-exit locations of PKP phase. Further, we omit anomalies in the upper mantle because PKP scattering in the upper mantle would be recorded after the PKIKP onset. We ignore the long wavelength P velocity variations due to the effect of thermal variations on V_P.

We use the AxiSEM method (Nissen-Meyer et al., 2014) (www.axisem.info) to compute body-wave seismograms up to 0.75 Hz. AxiSEM honors visco-elastic anisotropic Earth models van Driel and Nissen-Meyer (2014), but assumes that the seismic velocity structure has a rotational symmetry about the axis through the poles. We use the PREM model as the background model in all simulations. The earthquake source is a radially oriented monopole with nearly isotropic P radiation in the direction of the PKP and PKIKP waves. AxiSEM waveform simulations run on a 2D numerical section and do not account for out- of-plane scattering. They produce accurate 3D wavefields for 1-D models and models with in- plane lateral heterogeneities. The method is thus appropriate to produce accurate wave fields for the axisymmetric input models delivered by our thermochemical simulations. We analyze arrival times and amplitudes of PKIKP precursors using the same processing steps as described in Section 2.1. We align the synthetics on the peak-amplitude of PKIKP, normalize each trace so PKIKP has an amplitude of 1, and stack waveform envelopes.

To optimize sampling of the heterogeneous mantle (see Fig. 4) we calculate waveform stacks for four different earthquake locations. By rotating the 2D plane of wave propagation with respect to the source up 15° we attain near-uniform sampling of heterogeneity in the mantle by four bundles of PKP waves. As a consequence, all wave speed anomalies within the mantle sections contribute equally to our simulated images of PKP scattering. As an example, Fig. 6 shows the waveforms of PKIKP precursors and their stacked envelopes from four AxiSEM simulations with repositioned events for simulation *A*. The waveform differences are due to differences in scattering locations but the onset times and overall amplitude character as a function of distance is similar for each of the four simulations.

To simulate traveltime variability due to large-scale wavespeed heterogeneity we stack 4000 envelopes (not shown Fig. 6) of the same waveform after applying random traveltime shifts to the precursory window (time < 0 s). The traveltime shifts have a Gaussian distribution with a standard deviation of 1.5 s, corresponding to the recorded traveltime variation of PKIKP. The stacking of the slightly time shifted waveforms leads to smooth envelopes of PKIKP precursor waveforms. It has a negligible effect on the onset times and amplitude dependence on epicentral distance. In Fig. 6 we stack four envelopes without traveltime variations to show the effect of envelope smoothing.

3. Results

3.1. Effect of the strength of P velocity heterogeneity

The results in Fig. 7 show the effects of variations in P wave velocity perturbations δV_P for simulations *A* and *B* on the amplitude of PKIKP precursors. We use $\delta V_P = 0.1$ and 0.2%, with the lower value adapted from the analysis by Margerin and Nolet (2003) and Mancinelli and Shearer (2013). These δV_P values are consistent with mineral physics estimates Cobden et al. (2009). To facilitate the comparison with the data stacks from Fig. 3, we draw contours at PKIKP precursor amplitude 0.04, 0.1, and 0.25 for both the simulations and the data. The velocity perturbation δV_P affects the strength of PKIKP precursors most significantly in simulation *A*. Precursor amplitude is strongest between 134° and 137° for both *A* and *B* as is evident in the shifts of the 0.1 amplitude contours.

For simulation *A*, we obtained the best match to the recorded strength of PKIKP precursors for $\delta V_P = 0.2\%$, especially near an epicentral distance of 137°. When δV_P = 0.1% the simulated PKIKP precursors do not have the early high amplitude onset seen in the data at distances larger than 137°. For simulation *B*, the strength of the PKIKP precursors depends less strongly on δV_P. This indicates that the radial variation of *C* (see Fig. 5) controls the time and distance dependence of the PKIKP precursors more significantly than δV_P.

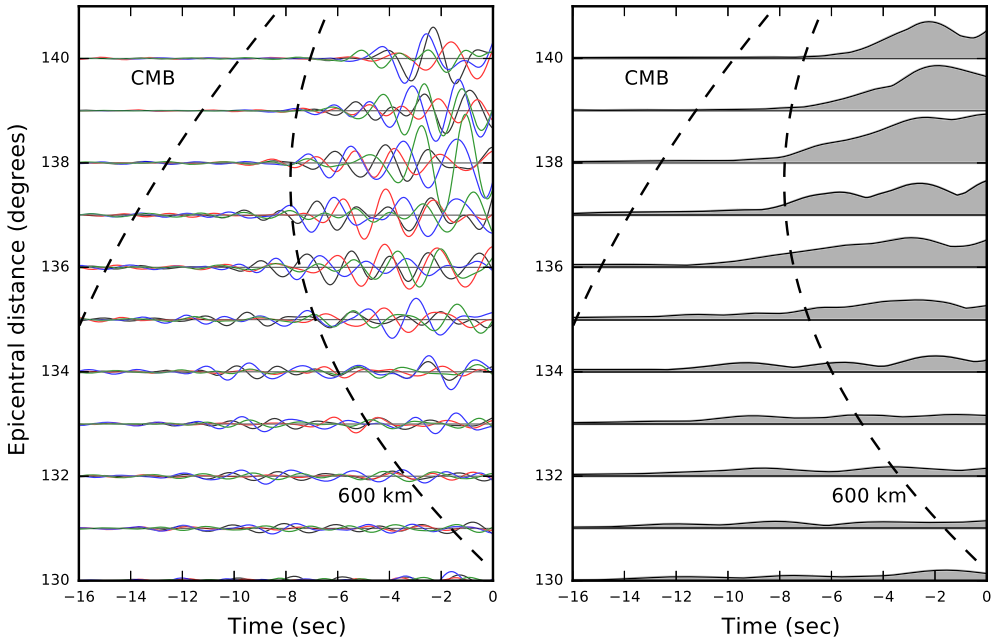

Fig. 6. Example of AxiSEM waveforms (left) and the waveform envelope (right). The PKIKP onset is at time = 0. Four waveforms (red, green, blue, and black) are computed for MORB profiles in the mantle at four different locations in simulation A. The dashed lines indicate the ray theoretical onset time of precursors due to scattering at the CMB and at 600 km above the CMB. (For interpretation of the references to color in this figure legend, the reader is referred to the web version of this article.)

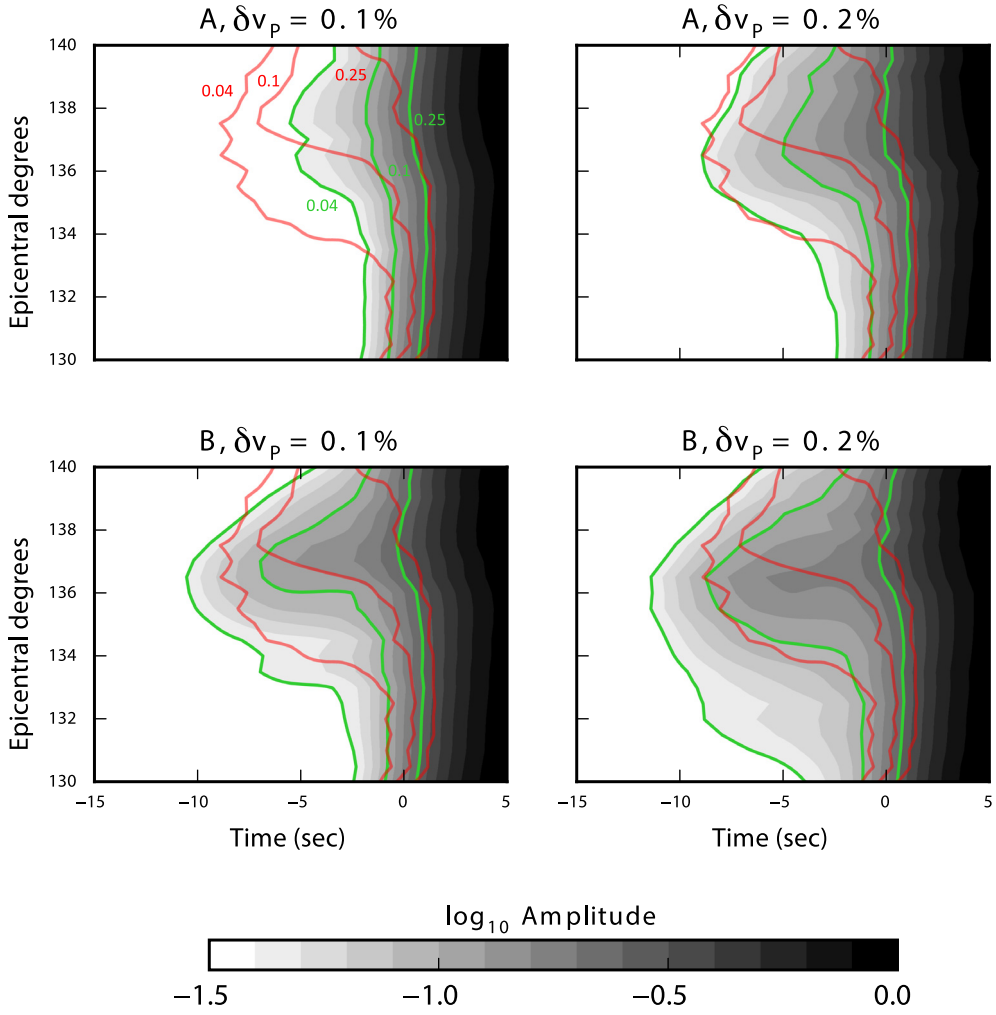

Fig. 7. Amplitude as a function of arrival time and epicentral distance of PKIKP precursors simulations *A* (top) and *B* (bottom) for $\delta V_P = 0.1\%$ (left) and $\delta V_P = 0.2\%$ (right). The PKIKP amplitude is 1 on the PKIKP onset is at time = 0. The green lines are the contours where the amplitudes are 0.04, 0.1, and 0.25. The red lines are contours where the amplitudes in the data are 0.04, 0.1, and 0.25. These are adopted from Fig. 3.

3.2. Effect of MORB distribution

Fig. 8 illustrates how the strength of PKIKP precursors depend on the assumed value for the excess density $\delta\rho$ of MORB with respect to the ambient mantle. MORB's excess density $\delta\rho$ determines its buoyancy and therefore its concentration C in the mantle. In the analysis of the simulations from Table 1 we assume that a MORB fragment corresponds to a P wave anomaly with $\delta V_P = 0.1\%$. The significant differences between the strength of PKIKP precursors between simulations *A* and *B* indicate that PKP scattering is strongly influenced by radial gradients in C (see Fig. 5). For simulation *A*, in which C does not change with depth, the PKIKP precursors are much weaker than in the data and do not have a clear early onset for distances larger than 136°. The PKIKP precursors simulated for *B*, when the MORB concentration increases fourfold in the lowermost mantle, match the amplitude and early high amplitude onset near 137° in the data.

For both *A* and *B*, the PKIKP precursor amplitudes are larger in the upwelling sections of the mantle (i.e., A_2 and B_2) than the downwelling (i.e., A_1 and B_1) sections of the mantle. Compared to A_1 and B_1, respectively, C is highest in the lowermost mantle for A_2 and B_2. The image of PKIKP precursors simulated for B_2 matches the recorded PKIKP precursors best, indicating that the concentration of small-scale heterogeneity increases strongly in the lowermost 500 km of the mantle. The effect of strong heterogeneity in the lowermost mantle on the onset of PKIKP precursors is apparent when comparing the simulations for A_1 and A_2 with the simulation for *A*. The narrow spikes in C at the CMB or 200 km above the CMB (see Fig. 5) produce the early onset of PKIKP precursors in comparison to *A*.

4. Discussion and conclusions

This paper describes initial results of combined geodynamic and waveform modeling of PKP scattering by small-scale heterogeneity in the lower mantle. We have used the mantle circulation simulations from Brandenburg et al. (2008) to map advected mid-ocean ridge basalt fragments as P velocity anomalies in the mantle and applied the spectral-element method AxiSEM (Nissen-Meyer et al., 2014) to determine their effects on high-frequency waveforms. We mapped the strength of PKIKP precursors, reflecting PKP scattering, using the global waveform stacking approach by Mancinelli and Shearer (2013) and Mancinelli et al. (2016).

Our simulations reproduce the onset time and strength of PKP scattering recorded in global seismic network data at frequencies lower than 0.75 Hz if we assume that P wave anomalies with dimensions of at least 20 km have a velocity contrast of 0.1% with respect to the mantle. This is consistent with previous estimates (e.g., Margerin and Nolet, 2003; Mancinelli and Shearer, 2013).

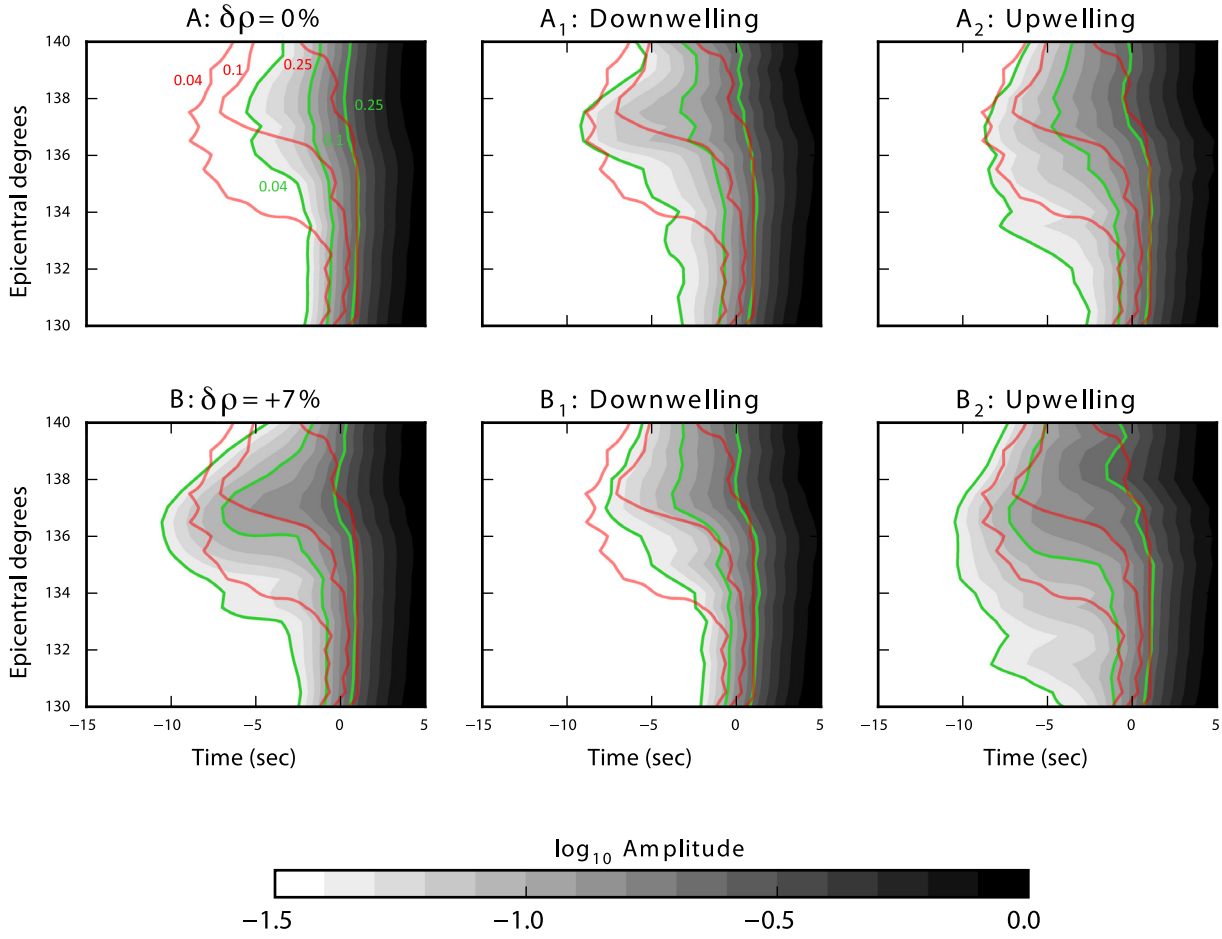

Fig. 8. Amplitude as a function of arrival time and epicentral distance of PKIKP precursors for simulations A, A_1, and A_2 (top) and B, B_1, and B_2 (bottom). In all cases, $\delta V_P = 0.1\%$. The PKIKP amplitude is 1. The green lines are the contours where the amplitudes are 0.04, 0.1, and 0.25. The red lines are contours where the amplitudes in the data are 0.04, 0.1, and 0.25. These are adopted from Fig. 3. (For interpretation of the references to color in this figure legend, the reader is referred to the web version of this article.)

Models in which the concentration of small-scale heterogeneity increases in the lowermost 500 km of mantle by a factor of 4–5 may reproduce most accurately the recorded onset and amplitude of PKIKP precursors between 130° and 140°. These models are consistent with the accumulation of relatively dense MORB above the core-mantle boundary. PKP scattering is predicted to be particularly strong in regions of the lower mantle where MORB has accumulated into thick piles unperturbed by recent subduction.

Important simplifications of our modeling are, for a large part, due to the limited computational resources affordable to us. They prohibit a detailed interpretation of our results. Our geodynamic simulations of mantle mixing are based in 2D cylinder geometry by assuming incompressibility. The mantle is assumed to be a mechanical mixture of harzburgite and MORB with a pyrolite composition. It does not include possible contribution to PKP scattering from compositional heterogeneity in the lowermost mantle due to incomplete early Earth differentiation (Labrosse et al., 2007) or the presence of silicate melts (Williams and Garnero, 1996).

Our waveform computations are restricted to frequencies lower than 0.75 Hz. This limits us to analyzing heterogeneity with scale lengths larger than about 20 km. Previous studies have demonstrated that PKP scattering is much stronger at frequencies as high as 1 Hz and that heterogeneities responsible for PKP scattering are as small as 10 km (e.g., Mancinelli et al., 2016). Moreover, our waveform simulations ignore out-of-plane scattering which is likely significant in the mantle (Thomas et al., 2009) and is an important component in PKIKP precursors (Mancinelli et al., 2016). Ignoring out-of-plane scattering will underestimate precursor amplitudes. Furthermore, our simulations include only core-exit scattering which may further underestimate precursor amplitudes.

New simulations, also for 3D scattering in 3D models with the novel AxiSEM3D methodology (Leng et al., 2016) or other 3D spectral-element packages (Komatitsch and Tromp, 2002) are useful to further explore geodynamic scenarios for the generation and distribution of small-scale heterogeneity in the mantle and address whether or not the distribution of small-scale heterogeneity in the lower mantle can be used to constrain the dynamics of the mantle.

Acknowledgments

The seismic data have been provided by the IRIS Data Management Center. This research has been funded by NSF grants EAR-1246700 to Peter van Keken and EAR-1644829 to Jeroen Ritsema. We thank Sebastian Rost and an anonymous reviewer for helpful comments.

References

Bataille, K., Flatté, S.M., 1988. Inhomogeneities near the core-mantle boundary inferred from short-period scattered PKP waves recorded at the Global Digital Seismograph Network. J. Geophys. Res. 93, 15057–15064.

Brandenburg, J.P., Hauri, E.H., van Keken, P.E., Ballentine, C.J., 2008. A multiple-system study of the geochemical evolution of the mantle with force-balanced plates and thermochemical effects. Earth Planet. Sci. Lett. 276, 1–13.

Cao, A., Romanowicz, B., 2007. Locating scatterers in the mantle using array analysis of PKP precursors from an earthquake doublet. Earth Planet. Sci. Lett. 255, 22–31.
Cleary, J.R., Haddon, R.A.W., 1972. Seismic wave scattering near the core-mantle boundary: a new interpretation of precursors to PKP. Nature 240, 549–551.
Cobden, L., Goes, S., Ravenna, M., Styles, E., Cammarano, F., Gallagher, K., Connolly, J. A.D., 2009. Thermochemical interpretation of 1-D seismic data for the lower mantle: The significance of nonadiabatic thermal gradients and compositional heterogeneity. J. Geophys. Res. Solid Earth 114, 1–17.
Cormier, V.F., 1999. Anisotropy of heterogeneity scale lengths in the lower mantle from PKIKP precursors. Geophys. J. Int. 136, 373–384.
Doornbos, D.J., 1978. On seismic wave scattering by a rough core-mantle boundary. Geophys. J. Int. 53, 643–662.
Frost, D.A., Rost, S., Selby, N.D., Stuart, G.W., 2013. Detection of a tall ridge at the core-mantle boundary from scattered PKP energy. Geophys. J. Int. 208, 1–17.
Haddon, R.A.W., Cleary, J.R., 1974. Evidence for scattering of seismic PKP waves near the mantle-core boundary. Phys. Earth Planet. Int. 8, 211–234.
Hedlin, M.A.H., Shearer, P.M., 2000. An analysis of large-scale variations in small-scale mantle heterogeneity using Global Seismographic Network recordings of precursors to PKP. J. Geophys. Res. 105, 13655–13673.
Hedlin, M.A.H., Shearer, P.M., Earle, P.S., 1997. Seismic evidence for small-scale heterogeneity throughout the Earth's mantle. Nature 387, 145–150.
Hwang, Y.K., Ritsema, J., van Keken, P.E., Goes, S., Styles, E., 2011. Wavefront healing renders deep plumes seismically invisible. Geophys. J. Int. 187, 273–277.
Komatitsch, D., Tromp, J., 2002. Spectral-element simulations of global seismic wave propagation-II. 3-D models, oceans, rotation, and self-gravitation. Geophys. J. Int. 150, 303–318.
Labrosse, S., Hernlund, J.W., Coltice, N., 2007. A crystallizing dense magma ocean at the base of the Earth's mantle. Nature 450, 866–869.
Leng, K., Nissen-Meyer, T., van Driel, M., 2016. Efficient global wave propagation adapted to 3-D structural complexity: a pseudospectral/spectral-element approach. Geophys. J. Int. 207, 1700–1721.
Maguire, R., Ritsema, J., van Keken, P.E., Fichtner, A., Goes, S., 2016. P- and S-wave delays caused by thermal plumes. Geophys. J. Int. 206, 1169–1178.
Mancinelli, N.J., Shearer, P.M., 2013. Reconciling discrepancies among estimates of small-scale mantle heterogeneity from PKP precursors. Geophys. J. Int. 195, 1721–1729.
Mancinelli, N.J., Shearer, P.M., Thomas, C., 2016. On the frequency dependence and spatial coherence of PKP precursor amplitudes. J. Geophys. Res. 121, 1873–1889.
Margerin, L., Nolet, G., 2003. Multiple scattering of high-frequency seismic waves in the deep Earth: Precursor analysis and inversion for mantle granularity. J. Geophys. Res. 108, 2514–2530.
Miller, M.S., Niu, F., 2008. Bulldozing the core-mantle boundary: localized seismic scatterers beneath the Caribbean Sea. Phys. Earth Planet. Inter. 170, 89–94.
Nissen-Meyer, T., van Driel, M., Stähler, S.C., Hosseini, K., Hempel, S., Auer, L., Fournier, A., 2014. AxiSEM: Broadband 3-D seismic wavefields in axisymmetric media. Solid Earth. 5, 425–445.
Niu, F., Wen, L., 2001. Strong seismic scatterers near the core-mantle boundary west of Mexico. Geophys. Res. Lett. 28, 3557–3560.
Ritsema, J., Deuss, A., Van Heijst, H.J., Woodhouse, J.H., 2011. S40RTS: A degree-40 shear-velocity model for the mantle from new Rayleigh wave dispersion, teleseismic traveltime and normal-mode splitting function measurements. Geophys. J. Int. 184, 1223–1236.
Shearer, P.M., 2015. Deep Earth structure–Seismic scattering in the deep Earth. In: Seismology and the Structure of the Earth. Treatise Geophys., vol. 1. Elsevier, Amsterdam, pp. 695–729.
Shearer, P.M., Hedlin, M., Earle, P.S., 1998. PKP and PKKP precursor observations: implications for the small-scale structure of the deep mantle and core. Geodyn. 28, 37–55.
Styles, E., Goes, S., van Keken, P.E., Ritsema, J., Smith, H., 2011. Synthetic images of dynamically predicted plumes and comparison with a global tomographic model. Earth Planet. Sci. Lett. 311, 351–363.
Thomas, C., Weber, M., Wicks, C.W., 1999. Small scatterers in the lower mantle observed at German broadband arrays. J. Geophys. Res. 104, 15073–15088.
Thomas, C., Kendall, J.M., Helffrich, G., 2009. Probing two low-velocity regions with PKP b-caustic amplitudes and scattering. Geophys. J. Int. 178, 503–512.
Vanacore, E., Niu, F., Ma, Y., 2010. Large angle reflection from a dipping structure recorded as a PKIKP precursor: Evidence for a low velocity zone at the core-mantle boundary beneath the Gulf of Mexico. Earth Planet. Sci. Lett. 293, 54–62.
van Driel, M., Nissen-Meyer, T., 2014. Optimized viscoelastic wave propagation for weakly dissipative media. Geophys. J. Int. 199, 1078–1093.
van Driel, M., Nissen-Meyer, T., 2014. Seismic wave propagation in fully anisotropic axisymmetric media. Geophys. J. Int. 199, 880–893.
van Keken, P., 2001. Cylindrical scaling for dynamical cooling models of the Earth. Phys. Earth Planet. Inter. 124, 119–130.
Vidale, J.E., Hedlin, M.H., 1998. Evidence for partial melt at the core-mantle boundary north of Tonga from the strong scattering of seismic waves. Nature 391, 682–685.
Waszek, L., Thomas, C., Deuss, A., 2015. PKP precursors: implications for global scatterers. Geophys. Res. Lett. 42, 3829–3838.
Wen, L., 2000. Intense seismic scattering near the Earth's core mantle boundary beneath the Comoros hotspot. Geophys. Res. Lett. 27, 3627–3630.
Wen, L., Helmberger, D.V., 1998. Ultra-low velocity zones near the core-mantle boundary from broadband PKP precursors. Science 279, 1701–1703.
Williams, Q., Garnero, E.J., 1996. Seismic evidence for partial melt at the base of Earth's mantle. Science 273, 1528–1530.
Yao, J., Wen, L., 2014. Seismic structure and ultra-low velocity zones at the base of the Earth's mantle beneath Southeast Asia. Phys. Earth Planet. Int. 233, 103–111.